Enhancement of Shear Transfer in Composite Deck with Mechanical Fasteners

Christopher McComb, M.S., EIT

c/o Department of Mechanical Engineering
Carnegie Mellon University
5000 Forbes Avenue, Scaife Hall
Pittsburgh, PA 15213
Email: ccm@cmu.edu
Phone: +1 (559) 859-8459

Fariborz M. Tehrani, Ph.D., PE, SP, PMP

Department of Civil & Geomatics Engineering
California State University, Fresno
2320 E. San Ramon Ave., MS/EE94, Room E196
Fresno, CA 93740

Abstract

Reinforced concrete construction and steel construction are two of the most common contemporary construction methods. Both methods make use of composite decks as floor systems and diaphragms. During the design of composite decks, the interaction between the steel deck and concrete slab is typically disregarded when calculating the strength of the composite diaphragm due to lack of complete shear transfer, as existing practices such as stamping are not effective to provide substantial composite action. This conservative assumption essentially results in non-efficient use of material. This paper presents a method for ensuring shear transfer through the use of conventional sheet metal screws, driven through the corrugated steel deck and embedded in the fresh concrete. This method is proposed for use in the field *between* formed steel beams. Both experimental and analytical studies support an increase in strength with the addition of embedded fasteners. Further, experimental results indicate an additional increase in strength with the addition of synthetic reinforcing fibers. The increase in strength with the addition of the fasteners is on the order of 100%. When fasteners are already in use, the addition of synthetic reinforcing fibers can increase strength on

the order of 10%. The ultimate deflection of enhanced deck is comparable to deck tested without fasteners, but the initial stiffness of enhanced deck is much higher.

Keywords: reinforced concrete, composite deck, fiber reinforcement, mechanical fasteners

---

1. Introduction

Reinforced concrete is a very versatile building material, composing structural elements from slab-on-grade foundations to diaphragms and columns for multi-story buildings. However, substantial time and money is spent constructing forms in which to pour the concrete, as well as in setting the reinforcing bars. Reinforcement detailing is also a time intensive process for concrete structures, due to strict requirements for size, spacing, and number of bars. This can result in rebar congestion, ultimately resulting in a structure that is time- and labor-intensive [1, 2]. Additionally, the finite nature of steel bars can introduce stress concentrations in the concrete section. Composite concrete deck is a composite of steel and concrete that remedies some of these inefficiencies. This method of construction typically uses both steel sheet and reinforcing steel bars to achieve sufficient strength and constructability. However, non-composite decks are not uncommon in practice, where the steel deck is primarily used to support the concrete while it cures. In this method of construction, the shear transfer between the metal deck and concrete slab is limited to frictional forces, which are negligible. Thus, the steel deck is typically not included in design calculations, because it is generally assumed that the concrete does not act as a composite with the deck. Of course, it is desirable that the composite action directly takes place between the concrete slab and steel joists. It is common practice to ensure composite action of concrete deck with hot-rolled steel joists. This is accomplished by welding studs to the top of the steel deck, and through to the joist below. However, this only ensures composite action near the joist itself not in between joists. In this approach, the metal deck supports the fresh concrete between joists during construction. Later, when concrete cures, the composite action between the hardened concrete and steel joists contributes to the bearing of service and ultimate loads. The contribution of metal deck at this stage is minimal due to lack of composite action. Nevertheless, the deck configuration may not allow removal of metal deck from the system.

Ensuring that the steel deck participates in composite action with the concrete would save on material costs by taking advantage of the presence of metal deck and improving the overall strength of the section.

It is recognized that the main difficulty in the design of composite concrete deck is the development of shear transfer between the two materials [3]. Typically, when composite action is desired for a steel beam beneath the composite deck, shear studs are welded through the steel deck to the steel beam beneath prior to pouring concrete. However, this method is not feasible between beams, due to the limited thickness of the steel deck. Indentations in the deck attempt to develop some shear transfer, but the depth of the indentations is usually not sufficient. Better shear transfer can be accomplished using principles well-developed in connection design for CFS [3]. Another means for ensuring shear transfer in steel-concrete composites included cutting and bending the steel deck to produce shear tabs [4, 5].

The use of simple steel fasteners (i.e screws and nails) to resist shear has been studied in a variety of media. In an application for resisting shear between cold-formed steel (CFS) and concrete, it was determined that important failure modes included flexure, pull-out, and shear [6]. Similar fasteners have been explored to resist shear in timber/concrete composites. In a set of experiments that examined a large variety of different shear connection designs for a composite timber/concrete flooring system, the highest performing connection utilized a cast-in-place screw [7]. In another experimental study, cast-in-place nailed connections were explored as a means of developing better timber/concrete composite action, resulting in increased efficiency of the composite section [8]. Further, steel fasteners have been used to resist shear in CFS/calcium-silicate framed wall panel systems [9]. In this application, it was noted that a large amount of energy was dissipated through the screwed connection during failure [9].

The primary aim of this research is to demonstrate the effect of sheet metal screws in resisting transverse shear in composite concrete deck (see Figure 1). It should be noted that the thrust of this work is intended to strengthen composite action in the region between steel joists. Further, this project sought to demonstrate the contribution of polypropylene fibers toward the strength of the embedded fasteners, and thereby the overall strength of the composite concrete deck. The key contributions of this paper include combined implementation of mechanical fasteners, lightweight aggregates, and polypropylene fibers, as well as a procedure to adjust numerical model of flexural testing.

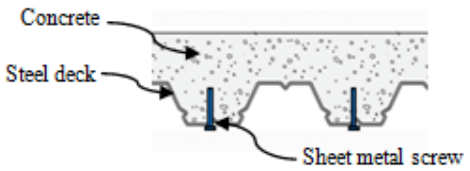

Figure 1: Placement of sheet metal screws

This paper is organized in four sections. First, the shear strength of the embedded sheet metal screws was determined experimentally. This was accomplished by loading symmetrical arrangements of embedded fasteners in shear and determining a load-deflection relationship. Second, the experimental data was used in a numerical model to predict the strength of a unit-width of enhanced composite concrete deck. Third, the numerical model was validated with a series of flexural tests. These tests involved loading short, unit-width spans of deck in four-point bending. Finally, a revised numerical model was developed that empirically accounted for interface friction at small deflections. This model could potentially act as a useful design tool for practicing engineers.

2. Concrete Mix Design

Table 1 details the mix proportions used in this research. These proportions were determined through a combination of absolute volume mix design and iterative modifications [10]. Mixes NWAP and NWAF contain normal-weight coarse aggregates, and mixes LWAP and LWAF contain lightweight coarse aggregate. Fine aggregates in all mixes have normal weight. It should be noted that the mix design in general practice varies based on required specified compressive strength, and thus, may differ from the mix design in this study. Therefore, projection of results to other types of concrete would require further experimental studies using appropriate mix design.

Table 1: Mix Proportions

Mix Designation	Coarse Ag.	Fine Ag.	Cement	Water	Fibers
LWAP	524 kg/m^3	837 kg/m^3	409 kg/m^3	218 kg/m^3	0 kg/m^3
LWAF	524 kg/m^3	837 kg/m^3	409 kg/m^3	218 kg/m^3	3kg/m^3
NWAP	1111 kg/m^3	777 kg/m^3	368 kg/m^3	138 kg/m^3	0 kg/m^3
NWAF	1111 kg/m^3	777 kg/m^3	368 kg/m^3	138 kg/m^3	3 kg/m^3

Two mixes contain polypropylene macro reinforcing fibers. These fibers are expected to control and limit shear cracking around the mechanical fasteners. Figure 2 shows a sample of these fibers. The fibers are approximately 5.5cm in length, round in cross-section, and approximately 1mm in diameter. The fibers are generally bunched in groups of 10 to 20 fibers, and are typically wavy. A dosage of 3 kg/m^3 (approximately 0.33% by volume) was recommended by the manufacturer for slab over metal deck construction [11].

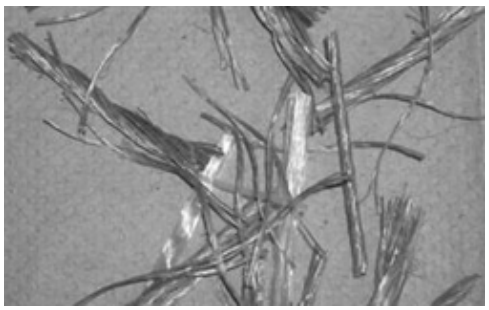

Figure 2: Polypropylene fibers

3. Embedded Shear Connection

The first portion of this work measured the shear strength of the cast-in-place sheet metal screw connection. This was accomplished with empirically-tested direct shear blocks. The dimensions of the cast-in-place sheet metal screw connection were designed to ensure that failure occurred in the concrete, thereby allowing the effect of fiber reinforcement to be determined during experimentation. The analysis considered rupture of the steel sheet, shear failure of the connector, breakout failure in the concrete, and pryout failure in the concrete. Pryout and breakout were analyzed according to standards in [12]. Shear failure of the screw was taken from manufacturer specifications, and rupture of the steel sheet was calculated according to standard methodology.

3.1. Apparatus and Specimen Construction

A total of five direct shear blocks were constructed for each of the mixes discussed previously. Figure 3 shows a typical specimen. Each specimen was constructed by first creating two sheet metal strips, measuring 5.1cm by 25.4cm (1.5mm thickness). A stainless steel sheet metal screw (6.3 mm in

diameter, and 3.2cm in length) was then driven through each sheet metal strip, as shown in Figure 3. This screw was driven into the sheet metal strip at a distance of 3.8cm from one end, and centered perpendicular to the axis of the strip. In order to facilitate attachment for loading, two holes (1.7cm in diameter) were then drilled in each sheet metal strip. They were located at distances of 2.5cm and 3.8cm, and also centered perpendicular to the axis. Finally, these sheet metal strips (or more accurately, the screws attached to the strips) were cast into a concrete block. This block measured 10.2cm $\times$ 10.2cm $\times$ 15.2cm. The screws were cast into opposite rectangular faces.

Figure 3: Direct shear block

Test fixtures were then created to allow the connections of the specimen to the loading apparatus. Figure 4a shows the general view of the top fixture. This fixture consists of a saddle in which the concrete block was allowed to sit. The fixture was composed of a bolt (intended to screw into the hydraulic actuator) and a piece of structural steel. The piece of structural steel had a cross section of 15.2cm$\times$20.3cm with a wall thickness of 9.5mm, and was cut to a length of 10.2cm.

Figure 4b shows the bottom fixture. This fixture allows the sheet metal strips to be attached using a pair of through bolts. The fixture consisted of a pair of 3mm thick steel plates (cut to fit and used as washers), and

structural steel piece. The piece of structural steel had a cross section of 10.2cm×10.2cm, with a wall thickness of 6.3mm, and was cut to a length of 10.2cm. All drilled holes were 1.6cm in diameter. The through bolts used to attach the sheet metal tabs to the lower fixture were made of 1.3cm threaded rod with matching nuts. Figure 4c shows the complete assembly, with direct shear block inserted and ready for loading.

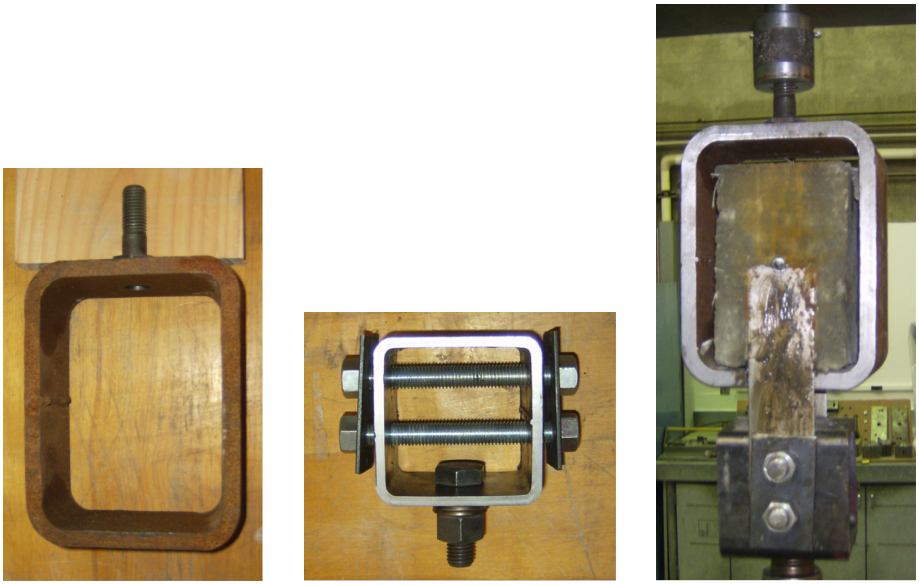

(a) Top fixture (b) Bottom fixture (c) Combined

Figure 4: Test fixture

3.2. Direct Shear Strength

The direct shear testing aims to capture the performance of embedded screws in the concrete section. Figure 5 shows the results of direct shear tests. Tests for the same mix are shown in the same figure. A minimum of two tests were performed for NWAP and NWAF mixes, and a minimum of three tests for LWAP and LWAF mixes. Figure 5 shows the raw experimental data from the tests, meaning that the data shown must be halved in order to correlate to the behavior of a single embedded screw. This is done later when the curves are idealized.

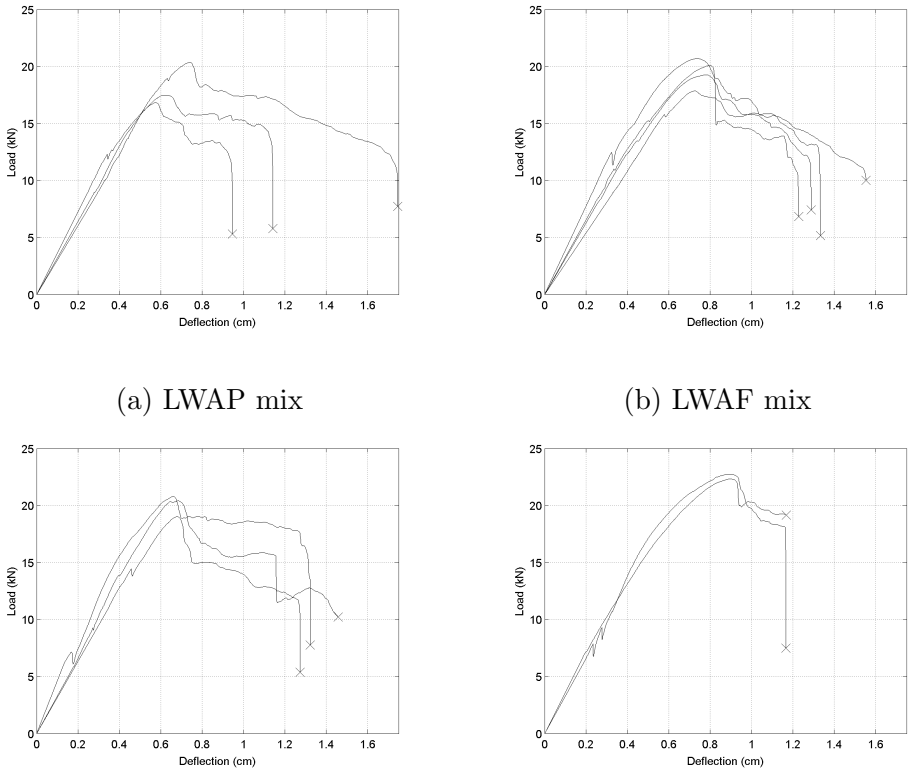

(a) LWAP mix

(b) LWAF mix

(c) NWAP mix

(d) NWAF mix

Figure 5: Direct shear block load/deflection curves

The tests shown in Figure 5a display a significantly larger amount of deviance than the other tests. This is attributed to the low shear strength of lightweight expanded shale aggregate. This aggregate is typically weaker than the cement paste matrix in which it is submerged, resulting in direct fracture and inconsistent ultimate strengths. The concrete strength for each mix design is shown in Table 2, along with a summary of the ultimate connection loads.

Table 2: Summary of Results for Direct Shear Tests

Mix Designation	Concrete Strength	Ultimate Connection Strength
LWAP	12.58 ± 2.39 MPa	9.11 ± 0.94 kN
LWAF	18.20 ± 1.81 MPa	9.74 ± 0.61 kN
NWAP	17.84 ± 4.15 MPa	10.46 ± 0.66 kN
NWAF	15.61 ± 3.74 MPa	10.97 ± 0.40 kN

In mixes utilizing both normal-weight and lightweight aggregate, the addition of fibers results in increased ultimate strength, and increased deflection at ultimate strength. The LWAF mix displayed increased ultimate deflection over the LWAP mix, but this behavior was not echoed in the NWAF and NWAP mixes. In contrast to the experiments in this work, typical welded shear studs maintain high post-yield strength. A more thorough discussion of behavior in welded shear studs can be found in [13].

The results in Figure 5 suggest that four distinct zones occur during the loading of the specimen. The first zone is a linear elastic region. The second zone is a plastic region, at the end of which the specimen reaches its ultimate strength. The third zone is a sudden drop, as pieces of the concrete in between the threads of the screw sustain substantial shear strains. The fourth zone indicates that the screw is being pulled out of the concrete. The first, third and fourth zones is modeled as a linear relationship, and the second zone is idealized as a parabolic curve. In order to fully define all of these zones, at least 6 distinct points are needed from each curve. The zones (numbered) and the points needed to define them (denoted by the lettered black circles) are shown in Figure 6.

Point a is located at the origin. Point b is located at 1/2 of the deflection of point d, because this is approximately where the load-deflection curves ceased to be linear. Point c is located at 3/4 of the deflection of point d, to allow for a quadratic curve to be fit along b-c-d. Point d is at the maximum load value of the curve. Point e occurs at the end of the drop that comes after the peak load is reached, and point f occurs at the maximum deflection of the test. These points were determined for every test, and values with the same mix design were averaged in order to yield a single curve for that mix. The average values were then used to produce the curves generated from them, as shown in Figure 7a and Figure 7b. A parabolic curve fit was applied to points b, c and d in order to smooth that region. These curves will be used to predict strength and deflection of composite deck that uses

these embedded fasteners.

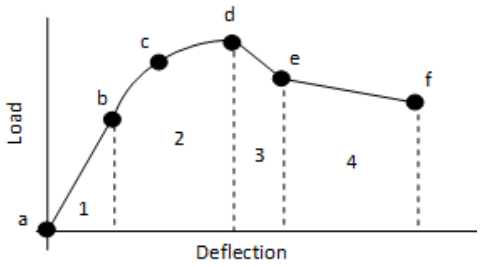

Figure 6: Idealized load/deflection relationship for direct shear blocks.

These points were determined for every specimen, and then averaged to produce mean values for a given mix.Figures 7a and 7b show these average load/deflection curves.

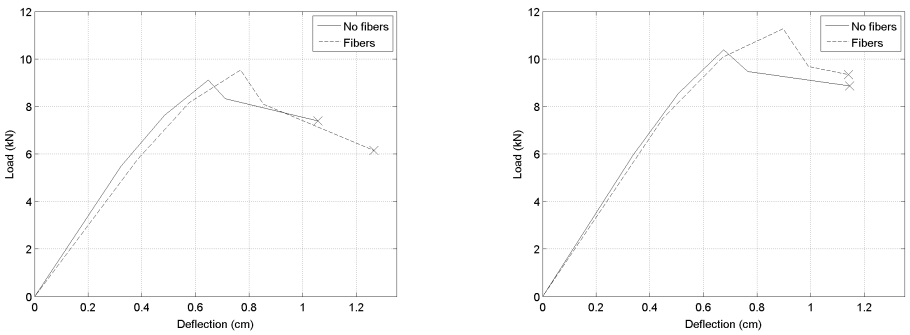

(a) LWAP and LWAF mixes (b) NWAP and NWAF mixes

Figure 7: Idealized direct shear block load/deflection curves

4. Flexural Analysis

The empirically developed load/deflection curves were then incorporated in a model to predict the performance of the enhanced composite deck. This section details the development of the model.

For reasons of numerical expedience, the concrete was idealized as being in a state of uniaxial stress. This then allowed the compressive stress-strain

behavior of concrete to be numerically described by the Hognestad curve [14]. This piecewise-defined function is defined as follows:

$$f_c = \begin{cases} f'_c \left(2\left(\frac{\varepsilon_c}{\varepsilon_0}\right) - \left(\frac{\varepsilon_c}{\varepsilon_0}\right)^2\right) & 0 \leq \varepsilon_c < \varepsilon_0 \\ f'_c \left(1 - Z(\varepsilon_c - \varepsilon_0)\right) & \varepsilon_0 \leq \varepsilon_c \leq 0.003 \end{cases} \tag{1}$$

where f'_c is the compressive strength of the concrete, the value of Z can be calculated as:

$$Z = \frac{0.5(f'_c - 6.89)}{\varepsilon_0(10.34 + f'_c)} \tag{2}$$

Equation 1 has been modified slightly from the original formulation. The value of ε_0 was set at 0.002 during computations because the concrete is unconfined [14].

The stress-strain curve of concrete can be extended for tensile stress if we consider concrete loaded in tension to remain elastic up to the point that it fractures (which is typical of most ceramic materials) [15]. After initial fracture, the material has a considerable amount of strength which consists of mechanical interlock between particles, and can be modeled as another linear segment [16]. We can describe the tensile stress as a function of strain with the following equation:

$$f_{c,t} = \begin{cases} E_c \varepsilon_c & 0 \leq \varepsilon_c < \varepsilon_t \\ -\frac{f_r}{4\varepsilon_t}\varepsilon_c + 1.25 f_r & \varepsilon_t \leq \varepsilon_c \leq 5\varepsilon_t \end{cases} \tag{3}$$

where ε_t can be calculated as follows:

$$\varepsilon_t = \frac{f_r}{E_c} \tag{4}$$

and where E_c is the elastic modulus of concrete, in MPa. This value is most accurately found with the ACI recommended equation [12]:

$$E_c = 0.043 w_c^{1.5} f_c'^{0.5} \tag{5}$$

where w_c is the mass density of concrete in kg/m^3 and f'_c is the compressive strength in MPa. The variable f_r stands for the modulus of rupture. The value of $0.6\sqrt{f'_c}$ is recommended by ACI, but the value is more accurately calculated as [17]:

$$f_r = 0.3 f_c'^{2/3} \tag{6}$$

where f'_c is given in MPa. Thus, for a concrete mix with compressive strength of 24 MPa and mass density of 2400 kg/m^3 we can derive the following stress strain curve shown in Figure 8.

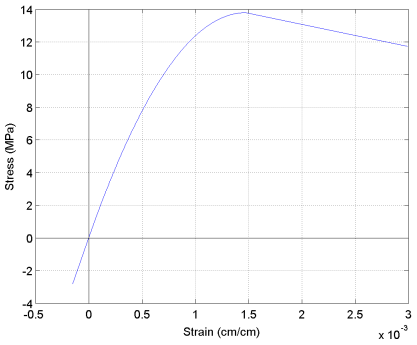

Figure 8: Theoretical stress strain curve for concrete compressive strength of 24 MPa and mass density of 2400 kg/m^3.

There are three common idealizations for steel stress-strain curves, with varying degrees of accuracy and complexity [18]. The idealization used for this project is a piecewise linear function defined as follows:

$$f_s = \begin{cases} E_S \varepsilon_s & 0 \leq \varepsilon_s < \varepsilon_y \\ F_y & \varepsilon_y \leq \varepsilon_s < 15\varepsilon_y \\ 482(\varepsilon_s - 15\varepsilon_y) + F_y & 15\varepsilon_y \leq \varepsilon_s < \varepsilon_u \\ \frac{0.1F_u}{\varepsilon_u - \varepsilon_f}\varepsilon_s + F_u\left(1 - \frac{0.1\varepsilon_u}{\varepsilon_u - \varepsilon_f}\right) & \varepsilon_u \leq \varepsilon_s \leq \varepsilon_f \end{cases} \tag{7}$$

where E is the elastic modulus of steel (200 GPa), F_y is the yield strength, F_u is the ultimate strength, ε_f is the elongation at failure, and ε_u and ε_y can be solved for as follows:

$$\varepsilon_y = \frac{F_y}{E_s} \tag{8}$$

$$\varepsilon_u = \frac{F_u - F_y}{482} + 15\varepsilon_y \tag{9}$$

where F_u is the ultimate tensile strength of the steel being considered. The stress-strain curve for steel is practically identical in tension and compression, so the same set of equations will be used for both. Using this

model, we can produce a stress-strain curve for steel conforming to ASTM A653 with a yield strength of 250 MPa and an ultimate strength of 475 MPa (see Figure9). This is the same steel used for many structural sheet steel products.

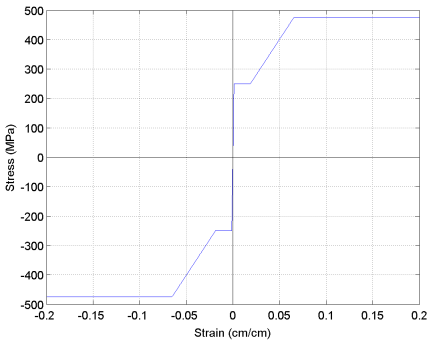

Figure 9: Theoretical stress strain curve for ASTM A653 steel

These material models were then combined with the shear connection strength model to calculate the strength of a given deck cross-section. The depth of the section was discretized into several horizontal slices (see Figure 10). A value for the strain at the top of the deck was then defined, and an iterative procedure was used to find the neutral axis (satisfying static equilibrium). The moment contributed from each strip was then summed to determine the moment strength for the chosen strain, and the curvature was calculated.

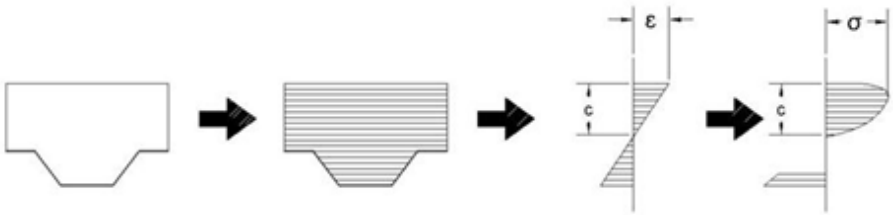

Figure 10: Discretization and force-summing scheme

The shear at the interface between the two materials was also considered. This was calculated in accordance with standard principals of mechanics of

materials. When calculating the moment of inertia a transformed section was utilized, disregarding all material that had failed. The shear per connector was then calculated based on the distance between connectors. Based on this load, the deflection at the connection was calculated based on the empirical relationship between load and deflection that was developed for embedded fasteners. This deflection was then incorporated into the curvature of the deck between fasteners. The deflected shape of the deck was determined by integrating the curvature function.

This model did not consider friction at the interface, because any frictional bond is usually broken at low strain values. Thus the metal deck is considered as a non-composite element. In addition, our modeling efforts do not account for rotation of the fastener within the concrete matrix.

5. Flexural Testing

5.1. Apparatus and Specimen Construction

Unit widths of the composite deck were constructed and tested. Each deck beam was 91.5cm long and had cross-sectional dimensions as shown in Figure 11.

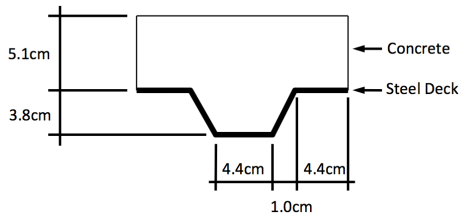

Figure 11: Cross section of composite deck unit width

These pieces then had stainless steel sheet metal screws driven through them. The screws were located in the center of the bottom web of the deck, and placed every 5.1cm. The first screw was placed 2.5cm from the end of each piece of deck. Each piece of deck then had approximately 5.1cm of concrete poured on top of it. This layout reflects a case in practice, where screws are repeated transversely at each rib. A total of 3 deck beams were prepared for each of the mix types, and 3 deck beams were also prepared with no sheet metal screws. These were prepared using plain lightweight

concrete. In order to distinguish shear failure from flexural failure, the deck beams were tested in four-point bending. Figure 12 shows the locations of the contact points.

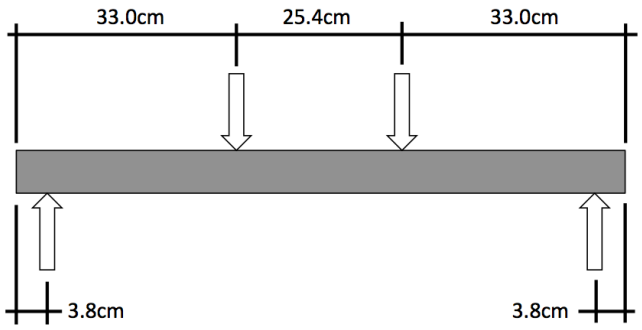

Figure 12: Four point bending diagram

5.2. Flexural Strength

Full results for the flexural test are shown in Figure **??**. The dashed lines indicate the predicted load-deflection behavior. Predictions were made using the model that was previously discussed. A large increase in capacity with the addition of sheet metal screws is shown in Figures 13b and 13d, when compared to Figure 13a. A further increase with the addition of reinforcing fibers is demonstrated in Figures 13c and 13e.

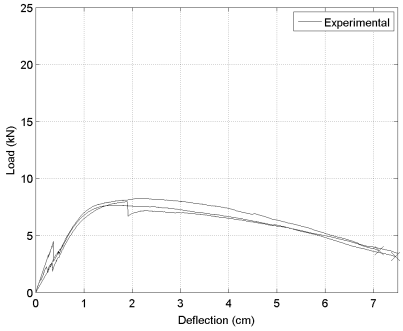

(a) LWAP without SMS

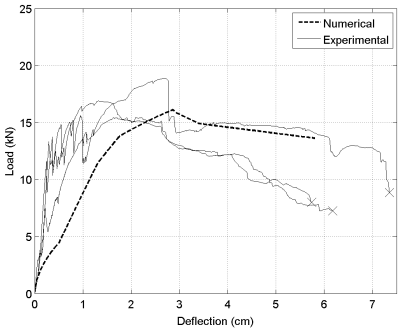

(b) LWAP mix with SMS

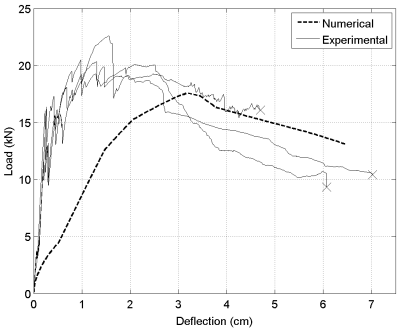

(c) LWAF with SMS

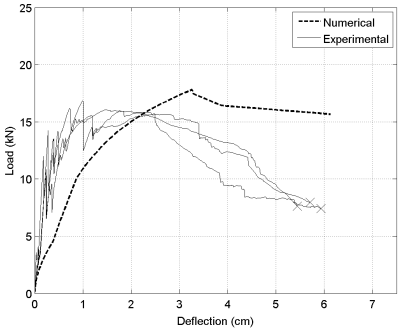

(d) NWAP with SMS

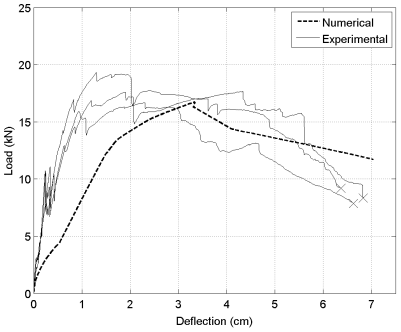

(e) NWAF with SMS

Figure 13: Flexural test load deflection curves

Almost all beams experienced a shear failure near one of the applied loads (see Figure 15a). A similar failure occurred in the beams without embedded fasteners, but the angle of failure was much higher, indicating a larger flexural component (see Figure 15b). Upon deconstructive inspection of the failure surfaces, it became apparent that each one of the cracks in the enhanced beams originated from an embedded fastener (see Figure 14). Predictions of the strength indicated that the fastener would fail in pullout. It appears that during loading the fastener had a torque applied to it, so that it acted as a pry-bar in the tensile region of the concrete, serving to induce the formation of cracks rather than pulling out.

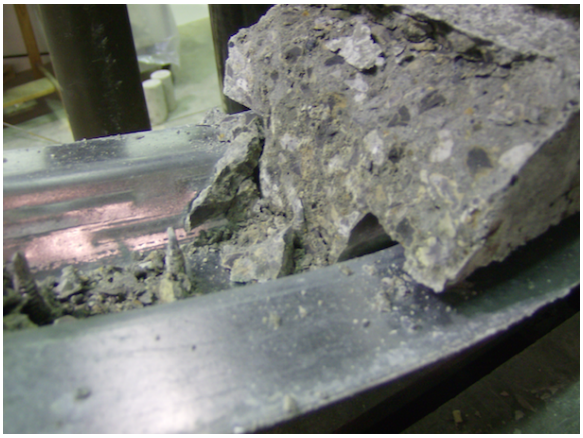

Figure 14: Shank of screw exposed at fracture surface.

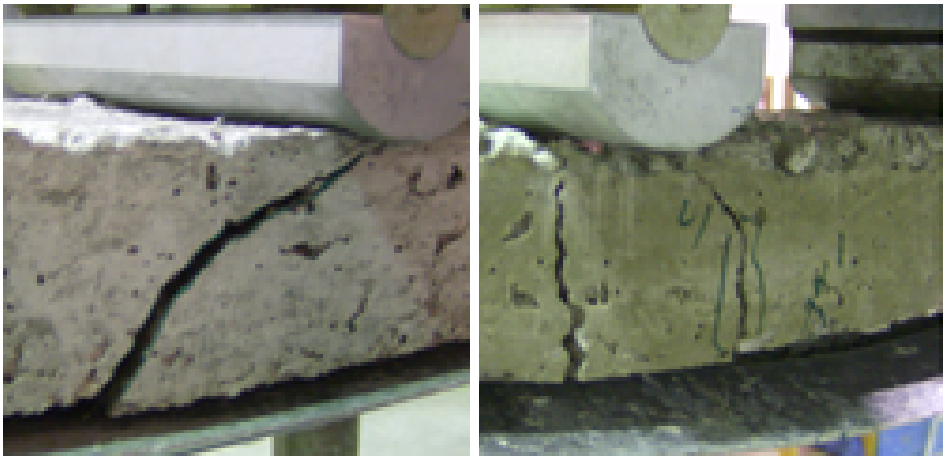

(a) With embedded fasteners (b) Without embedded fasteners

Figure 15: Typical failure modes

Despite this failure patterns, an obvious increase in load carrying capacity with the addition of embedded fasteners can be noted when observing Figures 13a and 13b. In addition, it is readily apparent that modest gains were made by the addition of fiber reinforcement. Table 3 shows the moment strength of the beams, pertaining to the maxima of the above curves as well as the predicted strength of the beams. The designation LWAPN denotes a series of beams tested with the LWAP mix, but without the addition of screws. Additionally, the average and standard deviation for the lightweight beams using fibers were calculated using the two lowest strengths, as the highest strength was determined to be an outlier.

Table 3: Flexural Results

Mix Designation	Concrete Strength	Ult. Flexural Strength	Predicted Strength
LWAPN	13.78 ± 0.11 MPa	1.16 ± 0.04 kN·m	1.06 kN·m
LWAP	13.78 ± 0.11 MPa	2.49 ± 0.25 kN·m	2.48 kN·m
LWAF	14.41 ± 0.23 MPa	2.96 ± 0.04 kN·m	2.71 kN·m
NWAP	15.37 ± 1.46 MPa	2.37 ± 0.08 kN·m	2.73 kN·m
NWAF	12.13 ± 1.64 MPa	2.61 ± 0.20 kN·m	2.44 kN·m

The predicted strengths in this table were determined using the model discussed previously. The number of discretized strips was 200 for every

prediction. The steel used for every prediction was identical (ASTM 653), but the stress-strain curve for the concrete was based on the compressive strengths of the test cylinders. The concrete stress-strain curve was not modified to account for matrix-fiber interaction.

The model was also used to predict the deflection of the span as a function of applied load (shown in Figure13b through 13e as a dashed line). In most of the figures, the predicted curve offered a good approximation of the actual behavior of the beams. However, the predictions fell short in several areas. First, in many cases the predicted maximum occurred at a deflection much higher than that of the experimental maximum. Second, the ultimate predicted deflection was often much lower than that measured experimentally. Third, the predicted strength immediately prior to failure was usually higher than that which was measured. These discrepancies can be primarily attributed to three phenomena which will now be discussed.

The first source of discrepancies between numerical and experimental results was the development of the load-deflection relationships for the embedded fastener. As noted previously, the primary failure noted for fasteners in the flexural tests was similar to breakout. However, the primary failure mode displayed during direct shear testing was pullout. Pullout was actually made nearly impossible during flexural testing, since the concrete was pushed into the steel deck by the applied load. Therefore, it is conceivable that the in-situ load-deflection relationship was slightly different than that which was developed separately. Principally, the in-situ relationship would have displayed greater ductility, limited mostly by the failure of the steel deck as the angle of the fastener changed (see Figure 16). In contrast, the failure during direct shear testing was usually a sudden pullout of one of the fasteners. This assists in explaining the discrepancy with respect to ultimate deflection.

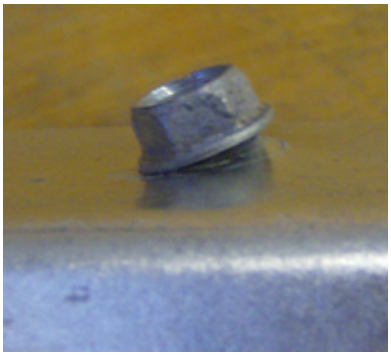

Figure 16: Head of embedded fastener, post failure.

The second source of discrepancies between numerical and experimental results was the change in cross-section of the steel deck during loading. After the peak load was reached, it was observed that the steel deck started to buckle. This is not anticipated to have a substantial impact on continuous decks, and therefore is not accounted for in conventional calculations. The top flanges of the deck buckled downwards, pulling away from the concrete and reducing the overall moment of inertia of the steel deck considerably. When actually installed, the non-symmetric buckling will be impossible since the deck will be continuous. It is estimated that during the post-peak loading of the deck, the moment of inertia of the steel alone dropped from 0.231 in^4 to 0.166 in^4, a total drop of 28%. For this reason, the real performance of the enhanced deck is expected to exceed the experimental performance.

The third source of discrepancies between numerical and experimental results concerns the fact that only a mechanical bond (the embedded fastener) was considered in the model to resist transverse shear between the concrete and the steel deck. In other words, both the chemical and frictional bonds were considered to be negligible. However, this was apparently not an accurate assumption. Initially, the experimental curves are quite stiff, indicating that for low deflection the friction between the steel and concrete plays an important role, and make the section act as a pseudo-perfect composite. This bond degrades as deflection increases, until the shear connectors are fully loaded. This indicates that the true performance could be more accurately resolved if the analytical model considered a region of full-composite action and a region of partially composite action, connected by a region displaying a transition between the two.

6. Revised Numerical Model

The model presented previously (developed from an analysis of the flexural capacity of the deck) indicated adequate predictive capabilities for the ultimate strength of the deck. However, the load-deflection relationship was not predicted well. A revised model is presented that modified the previous model in three ways. First, the deck was assumed to exhibit the effective composite stiffness up to half of the ultimate calculated load (this was based on observations of the experimental data). This was approximated as the full composite stiffness, multiplied by the ratio of available shear strength to shear strength required for full composite action. Second, after half of the ultimate load the stiffness of the deck was calculated as the average of two other stiffnesses: the initial stiffness of the previous model, and the initial stiffness of the composite section. Third, the section reached a strength plateau, until the point at which the previous model calculated a peak. This was also based on observations of the experimental data. The post-peak performance calculated using the last model remains unmodified. The experimental data along with the revised predictions are shown in Figure 17.

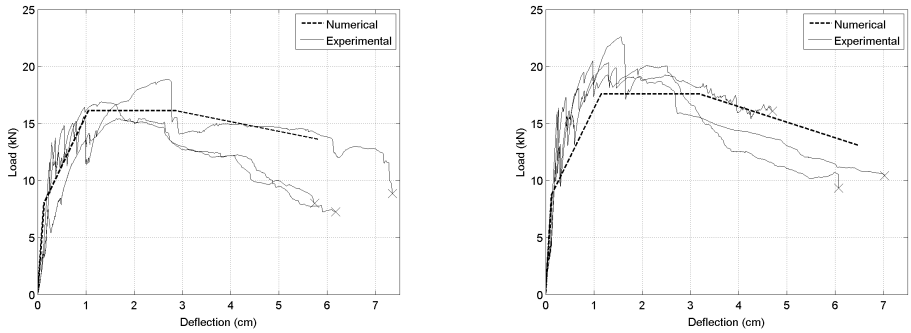

(a) LWAP mix with SMS

(b) LWAF with SMS

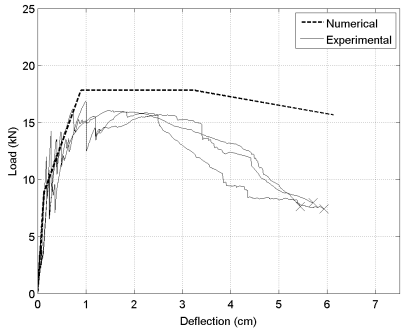

(c) NWAP with SMS

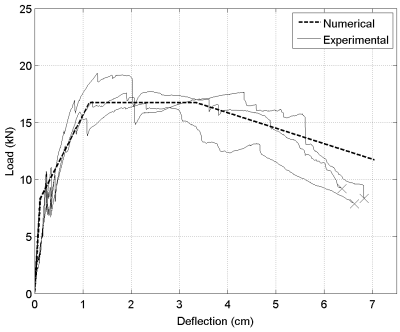

(d) NWAF with SMS

Figure 17: Revised model

Although this model does not offer high resolution, it resolves regions important for structural analysis and design (elastic, yielding, ultimate strength, and strain softening).

7. Conclusions

This project aimed to increase the strength of composite decks by increasing the shear transfer between the two materials. The results presented, both analytical and experimental, indicate that this can be accomplished by the use of embedded sheet metal screws, driven through the steel deck prior to pouring the concrete. For the purpose of this study stainless steel

sheet metal screws (6.3 mm in diameter, and 3.2cm in length) were driven at 5.1cm center-to-center spacing, with 5.1cm concrete cover. In the tests with lightweight concrete, the addition of sheet metal screws was shown to double the capacity of the deck. In addition, further gains can be realized with the addition of reinforcing fibers in the concrete. The addition of reinforcing fibers in the concrete was shown to increase the capacity of the deck by approximately 15% (in lightweight concrete) and by about approximately 10% (in normal-weight concrete).

The experimental results match up well with the analytical model. This model allows sufficient predictive capacities regarding the load-deflection behavior of the deck. Further, necessary adjustments in numerical model were discussed to validate tests, despite the size and boundary conditions of the specimens. Regardless, more experimental validation of the model is recommended. The experimental validation offered here only used a single fastener size, single fastener spacing, and single deck type. All of these variables must be explored and tested to determine the limitations of the analytical model. Moreover, the analytical model did not include the interaction between fibers and cementitious matrix. Such analysis will be part of future research plans.

Furthermore, it should be noted that the findings from this project have the potential for broad application. The process of driving sheet metal screws into steel deck is time intensive. Therefore, the method used in this project (i.e. that of driving the screws by hand) is suitable only for limited use. For example, the method might be used in locations where increased deck strength is beneficial in a specific and relatively small area. However, if this method were to be used for entire floors or roofs, it would be necessary to affix the screws (or a similar projection) using an automated manufacturing process. Stir-welding is a method which may prove particularly effective.

The outcome of this research warrants further studies on design parameters affecting the shear strength of the composite section, including the diameter of screws and the spacing between them; strength of concrete, deck, and screws; and fiber content, diameter, and length. While, the qualitative impact of these parameters on the shear performance of a composite section is well researched and understood, the quantitative approach to design of proposed section requires additional research.

Acknowledgements

The authors would like to thank Mr. Steve Scherer and Mr. Derick Gangbin for their assistance in construction and testing. The authors are grateful for material and services donated by the Utelite Corporation, the Forta Corporation, Verco Decking, Inc., Strategic Mechanical, Inc., Lehigh Hanson, and the Lyles College of Engineering. Partial funding was provided by Associated Students, Inc of California State University, Fresno.

References

[1] I. Vayas, A. Iliopoulos, Design of Steel-concrete Composite Bridges to Eurocodes, CRC Press, 2013.

[2] C.-K. Wang, C. G. Salmon, Reinforced concrete design, 1979.

[3] G. J. Hancock, Cold-formed steel structures, Journal of constructional steel research 59 (4) (2003) 473–487.

[4] J. M Irwan, A. Hanizah, I. Azmi, Test of shear transfer enhancement in symmetric cold-formed steel–concrete composite beams, Journal of Constructional Steel Research 65 (12) (2009) 2087–2098.

[5] J. Irwan, A. Hanizah, I. Azmi, H. Koh, Large-scale test of symmetric cold-formed steel CFS–concrete composite beams with BTTST enhancement, Journal of Constructional Steel Research 67 (4) (2011) 720–726.

[6] S. Erdélyi, L. Dunai, Behaviour of a new type of composite connection, Civil Engineering 48 (1-2) (2005) 89–100.

[7] B. L. Deam, M. Fragiacomo, A. H. Buchanan, Connections for composite concrete slab and LVL flooring systems, Materials and Structures 41 (3) (2008) 495–507.

[8] M. Taazount, S. Amziane, D. Molard, Tangential behavior of nailed composite timber–concrete floor structures, Construction and Building Materials 40 (2013) 506–513.

[9] M. Nithyadharan, V. Kalyanaraman, Experimental study of screw connections in CFS-calcium silicate board wall panels, Thin-Walled Structures 49 (6) (2011) 724–731.

[10] S. H. Kosmatka, W. C. Panarese, G. E. Allen, S. Cumming, Design and control of concrete mixtures, Vol. 5420, Portland Cement Association Skokie, IL, 2002.

[11] I. Forta, Applications: Slab on metal deck, Tech. rep.

[12] A. Committee, A. C. Institute, I. O. for Standardization, Building code requirements for structural concrete ACI 318-08 and commentary, American Concrete Institute, 2008.

[13] J. G. Ollgaard, R. G. Slutter, J. W. Fisher, Shear strength of stud connectors in lightweight and normal-weight concrete, AISC Engineering Journal 8 (2) (1971) 55–64.

[14] D. C. Kent, R. Park, Flexural members with confined concrete, Journal of the Structural Division 97 (7) (1971) 1969–1990.

[15] W. D. Callister, D. G. Rethwisch, Materials science and engineering: an introduction, John Wiley & Sons New York:, 2007.

[16] T. Yamamoto, F. J. Vecchio, Analysis of reinforced concrete shells for transverse shear and torsion, ACI Structural Journal-American Concrete Institute 98 (2) (2001) 191–200.

[17] F. Legeron, P. Paultre, Prediction of modulus of rupture of concrete, ACI Materials Journal 97 (2).

[18] H.-G. Kwak, F. C. Filippou, Finite element analysis of reinforced concrete structures under monotonic loads, Department of Civil Engineering, University of California, 1990.